J Neurophysiol 94: 2948–2958, 2005.
First published May 31, 2005; doi:10.1152/jn.00245.2005.

Controlling Synaptic Input Patterns In Vitro by Dynamic Photo Stimulation

Clemens Boucsein,[1,2,*] Martin Nawrot,[1,2,*] Stefan Rotter,[2,3] Ad Aertsen,[1,2] and Detlef Heck[1,4]

[1]*Neurobiology and Biophysics, Institute of Biology III and* [2]*Bernstein Center for Computational Neuroscience Freiburg, Albert-Ludwigs-University, Freiburg;* [3]*Institute for Frontier Areas of Psychology and Mental Health, Freiburg, Germany; and* [4]*University of Tennessee Health Science Center, Department of Anatomy and Neurobiology, Memphis, Tennessee*

Submitted 8 March 2005; accepted in final form 29 May 2005

Boucsein, Clemens, Martin Nawrot, Stefan Rotter, Ad Aertsen, and Detlef Heck. Controlling synaptic input patterns in vitro by dynamic photo stimulation. *J Neurophysiol* 94: 2948–2958, 2005. First published May 31, 2005; doi:10.1152/jn.00245.2005. Recent experimental and theoretical work indicates that both the intensity and the temporal structure of synaptic activity strongly modulate the integrative properties of single neurons in the intact brain. However, studying these effects experimentally is complicated by the fact that, in experimental systems, network activity is either absent, as in the acute slice preparation, or difficult to monitor and to control, as in in vivo recordings. Here, we present a new implementation of neurotransmitter uncaging in acute brain slices that uses functional projections to generate tightly controlled, spatio-temporally structured synaptic input patterns in individual neurons. For that, a set of presynaptic neurons is activated in a precisely timed sequence through focal photolytic release of caged glutamate with the help of a fast laser scanning system. Integration of synaptic inputs can be studied in postsynaptic neurons that are not directly stimulated with the laser, but receive input from the targeted neurons through intact axonal projections. Our new approach of dynamic photo stimulation employs functional synapses, accounts for their spatial distribution on the dendrites, and thus allows study of the integrative properties of single neurons with physiologically realistic input. Data obtained with our new technique suggest that, not only the neuronal spike generator, but also synaptic transmission and dendritic integration in neocortical pyramidal cells, can be highly reliable.

INTRODUCTION

Neurotransmitter release from a biologically inactive, or caged, precursor by means of light-induced photolysis has been used extensively for the mapping of functional connectivity in acute brain slices (Callaway and Katz 1993; Dalva and Katz 1994; Dantzker and Callaway 2000; Dodt et al. 2003; Katz and Dalva 1994). It is known as a method that is especially suitable to produce temporally and spatially defined neuronal activity in the slice tissue: the field of neurotransmitter release from the caged precursor is essentially confined to the diameter of the light beam (Dodt et al. 2003), and stimulus duration can be precisely controlled if a continuous light source with a fast shutter is used (Pettit et al. 1997). These features make photo stimulation not only a suitable method for functional mapping but can, in principle, be exploited to generate fast trains of postsynaptic depolarizations with a well-defined spatio-temporal structure. Such stimulation would allow one to study the impact of complex synaptic inputs on the physiological properties of neurons, under the tightly controlled experimental conditions of a slice preparation.

The importance of the intensity and the temporal characteristics of synaptic input for the physiological state of neocortical neurons has been increasingly recognized in recent years (for review, see Destexhe et al. 2003): Modeling studies have predicted dramatic changes in dendritic integration and input–output function of neurons under differently shaped synaptic input (e.g., Bernander et al. 1991; Destexhe and Pare 1999; Ho and Destexhe 2000; Kuhn et al. 2003, 2004; Salinas and Sejnowski 2000; for review, see Durstewitz et al. 2000), and experimental work in vivo has supplied invaluable information concerning state-dependent changes of excitatory postsynaptic potential (EPSP) summation, dendritic integration, and sensitivity to sensory input (Azouz and Gray 1999, 2000; Jagadeesh et al. 1993; Kamondi et al. 1998; Larkum and Zhu 2002; Leger et al. 2005; Pare et al. 1998; Stern et al. 2001; Zhu and Connors 1999). While the in vivo preparation is probably the most appropriate experimental model system to study the impact of network activity on single cells, it has major drawbacks, which are unlikely to be overcome in the near future: the accessibility of cells in vivo is limited, and the extent as well as the spatio-temporal characteristics of synaptic activity cannot be well controlled in the intact animal.

The acute slice preparation, on the other hand, offers excellent access to neuronal cells, as is shown by multiple intracellular recordings from the same cell (Larkum et al. 2001; Magee and Cook 2000; Oviedo and Reyes 2002; Williams and Stuart 2002), recordings from single synaptic boutons (Bischofberger et al. 2002), or up to quadruple recordings from closely neighboring, visually identified cells (Markram et al. 1998; Tamas et al. 2002). Vivid neuronal activity can be reintroduced into the otherwise largely deafferentiated slice by photolysis of caged neurotransmitters if a high number of spatially distributed postsynaptic sites are stimulated within short time windows. This is either achievable through a direct stimulation of distributed locations on the dendritic tree, or through the suprathreshold stimulation of cells presynaptic to the recorded neuron, which leads to synaptic input through functional projections onto the postsynaptic cell. Both approaches require that spatially distributed target sites can be stimulated in rapid succession, i.e., that the location of the stimulating light spot can be moved within milliseconds over a large portion of the slice.

In experimental setups conventionally used for photolysis of caged compounds, the UV light is introduced either through the objective of the microscope (Callaway and Katz 1993; Dodt et al. 1999; Kötter et al. 1998; Pettit et al. 1997; Wang

* C. Boucsein and M. Nawrot contributed equally to this work.

Address for reprint requests and other correspondence: C. Boucsein, Neurobiology and Biophysics, Inst. of Biology III, Albert-Ludwigs-Univ., Schänzlestrasse 1, D-79104 Freiburg, Germany (E-mail: clemens.boucsein@biologie.uni-freiburg.de).

The costs of publication of this article were defrayed in part by the payment of page charges. The article must therefore be hereby marked "*advertisement*" in accordance with 18 U.S.C. Section 1734 solely to indicate this fact.

and Augustine 1995) or through optical fibers inserted directly into the tissue (Godwin et al. 1997; Kandler et al. 1998; Margulis and Tang 1998). However, these methods are not suitable to change target location rapidly over a wide spatial range: target position changes in a setup where the light is focused through the objective require the movement of the entire microscope or, alternatively, the recording chamber, while optical fibers have to be repositioned by means of a micromanipulator. Systems that employ an acousto-optic device (Bullen and Saggau 1999) or galvanic scanning mirrors (Shepherd et al. 2003) for rapid deflection of a laser beam that is projected to the slice through low-power objectives have been described. However, their light-projection area is limited to the small field of view of the objective.

Here we describe a setup, developed to project the focused beam of a continuous argon ion UV laser through the bottom of the recording chamber directly onto the slice. It allows us to reach any desired target location within the entire chamber in <1 ms and, thereby, to introduce vivid synaptic activity into acute brain slices with a well-defined and tightly controlled spatio-temporal pattern. Our aim was to employ the activation of functional synaptic projections, rather than direct stimulation of the postsynaptic cell, because we wanted the synaptic input to be as realistic as possible. This approach has additional advantages: it avoids photo damage of the cell in which the activity-dependent mechanisms are being studied as well as unwanted effects of local accumulation of released neurotransmitter close to this cell. Glutamate accumulation can lead to the activation of extrasynaptic glutamate receptors, which will not only distort the electrical responses but can also trigger apoptosis in neurons (Hardingham et al. 2002).

In this study, we show that our setup is a suitable tool to elicit postsynaptic currents (PSCs) in neocortical pyramidal cells from purely synaptic origin with high reliability and precision. We also exemplarily applied a barrage of PSCs generated by the stimulation of presynaptic neurons for tens of seconds and quantified the reliability of the postsynaptic response for the repeated presentation of the same stimulus sequence. The results suggest that signal transfer between neurons in neocortical tissue can be highly reliable, even if the combined jitter introduced by synaptic transmission, dendritic integration, and action potential generation is taken into account.

METHODS

Dynamic laser stimulation: principle of operation

In our setup, the laser beam is introduced from below, through the bottom of the recording chamber (Fig. 1). The main advantages of this arrangement are *1*) the wide spatial projection range, which is not limited by an objective but covers the entire recording chamber, *2*) the fact that the laser beam does not run through a layer of buffer containing caged compound before it reaches the neuronal tissue, and *3*) that the tissue is not shaded from the laser beam by recording electrodes. We achieved target repositioning through two fast scanning mirrors that could direct the beam within <1 ms to any desired

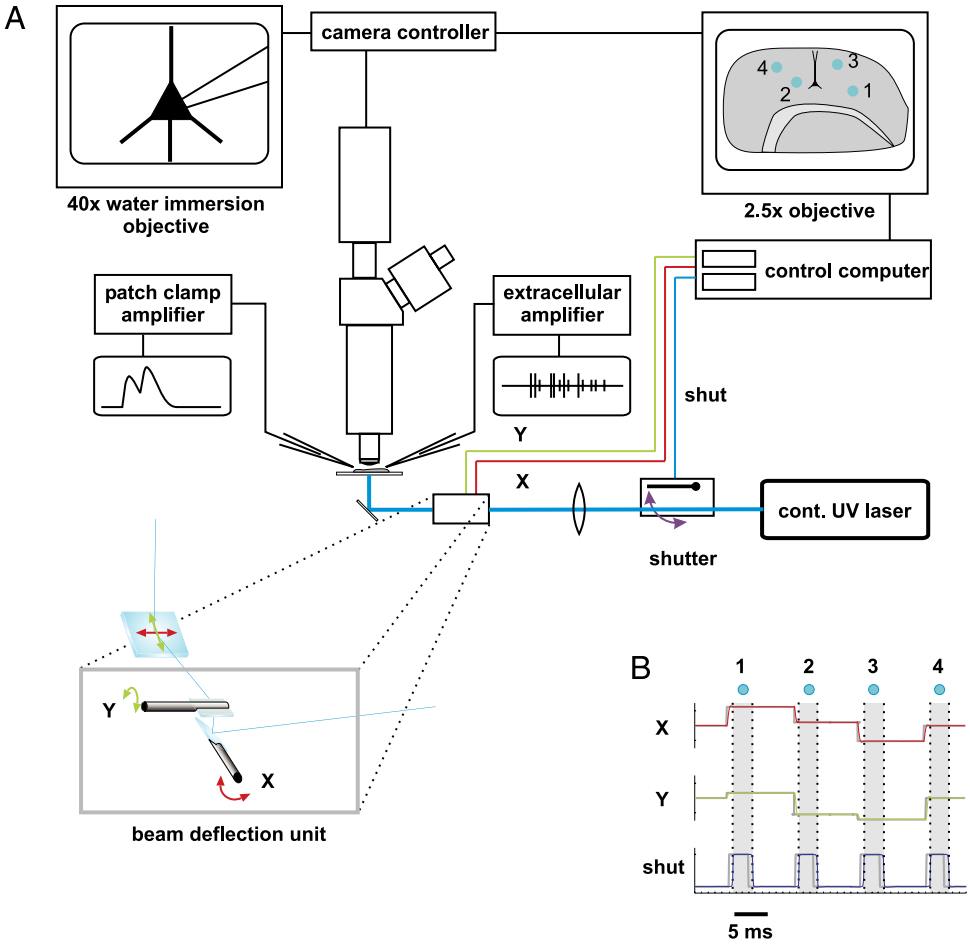

FIG. 1. *A*: schematic diagram of the setup for dynamic photo stimulation. A conventional fixed-stage upright microscope is equipped with an in vitro recording chamber that has a UV-light permissive quartz-glass bottom, through which the laser beam for photolytic release of the caged compound is projected onto the tissue. Beam deflection is achieved through 2 scanning mirrors (*inset*). A 3rd mirror is used to redirect the laser beam into the recording chamber and replaces the condenser required for high magnification IR video microscopy to establish the single-cell recording. During dynamic photo stimulation, the slice can be observed through a long distance, low magnification objective (×2.5). Light pulse duration is controlled by means of a programmable shutter. *B*: time-course of mirror and shutter movements. A feedback control signal provided by each of the galvanic scanner elements allows a precise on-line monitoring of the actual target position X (red) and Y (green) and of the open and close times of the shutter (blue). Gray curves represent the respective command signals issued by the control computer. Numbers refer to different stimulated target positions during 4 completed duty cycles, as symbolized in the low magnification sketch in the *top right corner* of *A*.

position within the entire recording chamber, with a spatial precision of >2 μm. Light pulse duration was controlled by a variable shutter with a response time of 0.8 ms. This arrangement allowed a duty cycle with a minimum duration of <4 ms, accounting for beam repositioning, shutter opening, 1-ms exposure, and shutter closure. It thereby enabled the stimulation of ≤300 spots/s at arbitrary locations.

Laser optics and beam deflection

The output power of the continuous wave water-cooled argon ion laser (ENTC II 652, Coherent, Santa Clara, CA) with two emission lines at 351.1 and 363.6 nm could be adjusted continuously, ranging nominally from 0 to 100 mW. Direct power measurements yielded an actual maximum output power of 108 mW. The laser beam with a diameter of ~1 mm was focused to a spot of about 50 μm diam in the plane of the slice tissue by an arrangement of two lenses (Fig. 1). Beam diameter refers to a drop below 10% of maximum power density, assuming a Gaussian beam intensity profile. To reduce power loss of the zoom optics to <8%, the input lens (plane-concave, $f = -40$ mm) and output lens (plane-convex, $f = 80$ mm) were optimized for near UV light. All mirrors were coated (Laser Design, Essen, Germany) and yielded a reflectance >99% for 45 ± 8° angle of incidence. The quartz glass recording chamber bottom added ≅2% power loss, leading to an accumulated power loss of the system of ~12%. All values for laser power (P) in this manuscript refer to nominal output power. Less than one-half of the 100-mW maximum laser power was usually required to release sufficient amounts of the caged compound within <10 ms at a concentration of 400 μM of caged glutamate in the bath solution.

The two scanning mirrors were mounted on temperature-stabilized galvanometric scanners (050 EFT, Laser-Scanning-Keiser, Stallikon, Switzerland) driven by appropriate control units (st150). The angular precision of about 1/300° (specification by manufacturer) resulted in a target resolution >2 μm. Beam deflections in angular coordinates (Θ; Φ) were converted into target translocations from the origin (Δx; Δy)according to

$$\Delta x \propto \tan\Theta \cdot \cos^{-1}\Phi \text{ and } \Delta y \propto \tan\Phi \quad (1)$$

which is approximately linear for small angles Θ and Φ

$$\Delta x \propto \Theta \text{ and } \Delta y \propto \Phi \quad (2)$$

For angles <2° covering a target area of about 5 × 5 mm^2, sufficient for typical slice experiments, the errors caused by this linear approximation were computed to be <2.5 μm in x and <1 μm in y. Analog voltage commands for control of the galvanometric scanners were issued through a 12-bit D/A converter (PCI-6711, National Instruments, Austin, TX) and linearly translated into rotation angle according to *Eq. 2*. The time τ for settling to a new angular position starting from rest was mainly determined by the inertial mass of the mirrors ($m \cong 1.5$ g, $\tau < 1$ ms) and the shutter plate ($\tau \cong 800$ μs), and thus essentially independent of rotation amplitude. To deliver the laser beam to the slice, the tilt-out infrared light condenser (U-SC 2, Olympus, Hamburg, Germany) used to establish the electrophysiological recording was swayed backward and replaced by a mirror mounted at 45° on a custom-made precision sledge (Fig. 1). It deflected the horizontally oriented beam coming from the scanning mirrors vertically toward the bottom of the recording chamber. To monitor wide regions of the slice, the ×40 water-immersion objective was replaced by a low magnification, long distance objective (×2.5). Illumination pulses could be monitored as blue emission caused by auto-fluorescence of the tissue.

Animals and preparation of brain slices

Long-Evans rats (P17–P25) were anesthetized with isofluran and decapitated. Brains were quickly removed and transferred to ice-cold preparation buffer containing (in mM) 217 sucrose, 2.5 KCl, 1.25 NaH_2PO_4, 7 $MgCl_2$, 0.5 $CaCl_2$, 25 $NaHCO_3$, and 10 glucose, pH 7.4. Slices of 350 μm thickness were cut with a vibratome (DT 1000, Dosaka, Japan) and stored at 33°C for 1 h in a storage solution containing (in mM) 125 NaCl, 2.5 KCl, 7 $MgCl_2$, 0.5 $CaCl_2$, 25 $NaHCO_3$, 1.25 NaH_2PO_4, and 25 glucose, pH 7.4, gassed with carbogen. For electrophysiological recordings, slices were transferred to a custom-made recording chamber of an upright microscope (Olympus BW51). Animal treatment was according to the Freiburg University's and German guidelines on the use of animals in research. All chemicals were purchased from Sigma (Deisenhofen, Germany) if not otherwise noted. TTX and the metabotropic glutamate receptor blocker (*RS*)-α-methyl-4-carboxyphenylglycine (MCPG) were purchased from Tocris (Köln, Germany).

Electrophysiological recordings

Whole cell patch-clamp recordings from layer V pyramidal cells in coronal slices of the somato-sensory cortex were established using infrared video microscopy (Dodt and Zieglgansberger 1990). Population activity in the slice was monitored with extracellular recordings at varying sites (1 or 2 independent electrodes). All recordings were performed at 30–34°C in a submerged-type chamber constantly superfused with artificial cerebrospinal fluid (ACSF) composed of (in mM) 125 NaCl, 2.5 KCl, 1 $MgCl_2$, 2 $CaCl_2$, 25 $NaHCO_3$, 1.25 NaH_2PO_4, and 25 glucose, pH 7.4, gassed with carbogen at a flow rate of 2–6 ml/min. For patch-clamp recordings, pipettes were pulled from thin-walled borosilicate glass (2 mm OD with filament; Hilgenberg, Malsfeld, Germany) on a horizontal Flaming-Brow puller (P97, Sutter Instruments, Novato, CA) to a resistance of 3–7 MΩ and filled with a solution containing (in mM) 140 K-gluconate, 10 HEPES, 2 $MgCl_2$, 2 NaATP, 10 EGTA, and 0.1% biocytin, adjusted to pH 7.3 with KOH. Pipettes for extracellular recordings were pulled to a resistance of 200–600 kΩ and filled with ACSF. Electrophysiological signals were recorded with conventional electronics (intracellular: Axoclamp 2B or AxoPatch 200A, Axon Instruments; extracellular: model 1800, A-M Systems, Everett, WA), digitized at 12–25 kHz with a CED 1401 Plus A/D converter (Cambridge Electronic Design, Cambridge, UK), and stored using Spike2 software (CED). Liquid junction potentials were not corrected for. Extracellular data were band-pass filtered (100 Hz to 3 kHz), whereas intracellullar data were low-pass filtered at 3–5 kHz. In addition, voltage-clamp recordings were low-pass filtered off-line at 2 kHz for PSC analysis. Statistical analyses were performed using Matlab (Mathworks, Natick, MA).

For recordings during dynamic photo stimulation, γ-CNB-caged L-glutamic acid (G-7055, Molecular Probes, Leiden, Netherlands) was added to 5 ml of ACSF to yield a concentration of 400 μM, which was circulated. Recycling of the caged compound was necessary to keep costs at an acceptable level. An alternative way to lower caged glutamate consumption would be to substantially reduce the flow rate of the ACSF. However, a high superfusion speed is desirable to allow for a fast supply of new caged compound, oxygen, and glucose, and removal of uncaged neurotransmitter. Obviously, recycling of the caged compound carries the risk of accumulating free glutamate in the superfusate. Wash-in of preused caged glutamate solution showed, however, that there was no detectable effect of putative free glutamate, even after several stimulation cycles. To prevent the activation of extrasynaptic metabotropic glutamate receptors, which can mediate apoptotic events in pyramidal neurons (Hardingham et al. 2002), the unspecific metabotropic glutamate receptor antagonist (*RS*)-MCPG (500 μM) was added to 5 ml of circulating ACSF containing the caged compound. This increased the survival time of the tissue but was no essential prerequisite to evoke vivid synaptic activity.

(*RS*)-MCPG could thus be omitted in experiments where it is crucial to keep the metabotropic glutamate receptors functional.

Histology and reconstruction of cell morphology

After recording, slices were fixed in 4% paraformaldehyde over night, stained with standard procedures using the avidin-biotin complex reaction (Vectastain, Burlingame, CA) and DAB (Horikawa and Armstrong 1988), and transferred to gelatin-coated slides. Dehydration in an ascending alcohol row was followed by overnight incubation in benzoic acid methyl ester (Roth, Karlsruhe, Germany) and embedding in DPX. Camera lucida drawings of the stained cells were made using a conventional microscope equipped with a camera lucida module (Dialux22, Zeiss, Oberkochem, Germany).

Statistical analysis

To quantify population spike activity, extracellular voltage signals were first rectified and then filtered using a first-order low-pass with a time constant of 15 ms. The response to a single light pulse was measured during the 200 ms after pulse onset, whereas a baseline value of the average over the 50 ms preceding the pulse was subtracted. Population response area refers to the integrated response, whereas population response amplitude was measured as the peak amplitude of the rectified and filtered signal (see sketch in Fig. 2*B*). For the detection of PSCs in the postsynaptic cell, a threshold of five times the SD of the membrane current during the 50 ms preceding the stimulus was applied. Reliability of stimulation was assessed by the percentage of trials that resulted in a detectable excitatory postsynaptic current (EPSC). For stimulations where EPSC amplitudes were close to detection threshold, reliability may be slightly underestimated because of false negatives. For quantifying the variability of PSC amplitude we computed the CV, i.e., the SD of amplitudes measured across repetitions, normalized as the mean amplitude. Temporal precision of the postsynaptic arrival of PSCs was measured as the SD of PSC onset time, defined as the time of threshold crossing. Reproducibility of the membrane potential dynamics as recorded during repeated stimulation sequences (Fig. 6) was evaluated as follows. First, we determined the peak times of all postsynaptic action potentials in all repetitions. Second, we removed the data within ±20 ms around peak time of each individual AP from each of the trials. We computed the cross-correlation between any pair of trials as a function of the relative time lag. To quantify the temporal precision with which action potentials were generated in the postsynaptic cell, we measured SD across repetitions of the spike peak times (in case of bursts, only the leading spikes were considered).

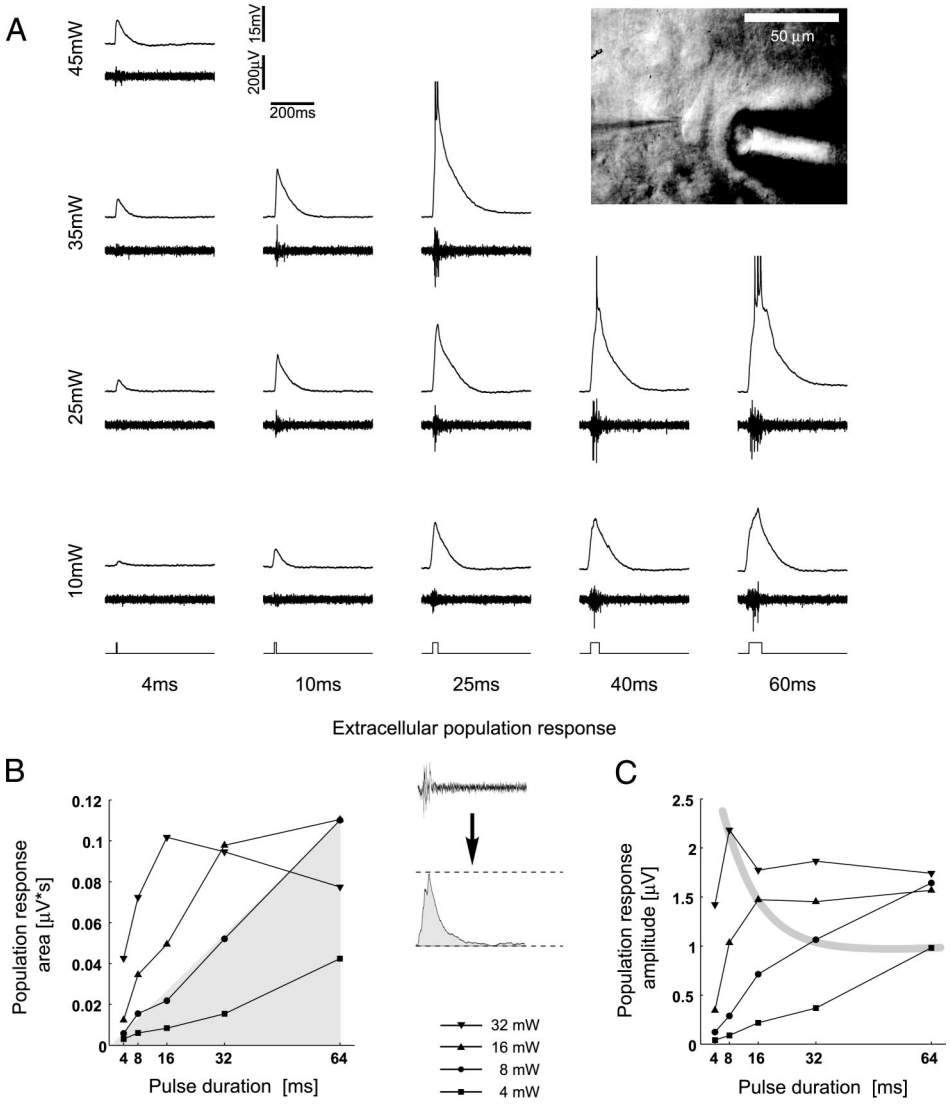

FIG. 2. Calibration of laser power and pulse duration. Both parameters allowed to fine-tune physiological responses to glutamate uncaging. *A*: intracellular responses to single light pulses centered at the soma of the recorded cell (*photo inset*) are displayed in the *top traces* (action potentials clipped), whereas multi-unit activity picked up by a nearby extracellular recording electrode is indicated by the *bottom trace* of each panel. Stimulus onset and duration are visualized by the traces in the *bottom row*. *B*: quantification of the extracellular population response area reveals that, for low laser power, total response during 200 ms after each single shot scales linearly with pulse duration. For high laser power, response saturates quickly with increasing pulse duration. *C*: peak amplitude of population response saturates at lower light intensities compared with response as measured by area. Taking peak amplitude as a measure of synchronicity of the recorded spike volley, calibration curve provides the means to select stimulus parameters with a prescribed degree of temporal clustering in population activity evoked by single pulses. Gray line indicates 0.25-mJ iso-cline for light energy introduced by a single stimulus pulse (product of pulse duration and laser power; curve fit by eye).

RESULTS

Presynaptic responses

In most experiments, our aim was to avoid direct photo stimulation of the cell in which the activity-dependent phenomena were to be studied. In this paper, we refer to this cell as the postsynaptic or intracellularly recorded cell. For the calibration of the stimulation parameters for presynaptic spike generation, however, intracellular recordings were performed from cells whose soma or dendrites were directly stimulated with light pulses of different intensities, durations, and spatial locations. These intracellular calibration measurements helped us to better interpret the results from recordings of the presynaptic population activity as measured with extracellular electrodes. They should not be confused with intracellular recordings from cells whose synapses were activated by spikes generated in presynaptic target cells.

For the first calibration measurements, solitary light pulses of different durations and intensities were applied to a single location, while the spike response from the neuronal population at that location was recorded with an extracellular electrode. At the same time, an intracellular recording from one of the neurons was employed to monitor subthreshold reactions to the photolytic release of glutamate (Fig. 2*A*). Quantitative analysis of the evoked population responses revealed that, while keeping the UV light energy per shot constant, population responses with quite different characteristics could be generated, depending on the particular combination of pulse duration and laser power. In general, increasing light intensity and decreasing pulse duration led to responses with higher amplitude, indicative of more synchronized activity, whereas longer pulses of lower intensity produced a smaller, more sustained response (Fig. 2, *B* and *C*). The subthreshold potentials measured with the intracellular recording showed that latency to spike generation and the number of spikes elicited in a single cell similarly depended on the combination of laser power and pulse duration (see Fig. 2*A*, *top traces*).

In a second set of calibration measurements, we determined the maximum stimulation frequency for a single location to study a possible shut-off of the responses by desensitization of glutamate receptors or depolarization block of the stimulated neurons. For that, we applied trains of 10 consecutive pulses with different interpulse intervals (IPIs) and quantified the population responses as described above. We found that the amplitude of the population response to consecutive pulses showed a reduction down to 70% of the response to the first pulse for IPIs in the range between 5 s and 500 ms, the effect being stronger at shorter IPIs. However, when the IPIs were further reduced to 200 ms or less, response amplitudes reduced less with increasing stimulation number (Fig. 3). For very short IPIs (close to pulse duration), responses to the single shots overlapped and were not distinguishable anymore. These data suggest to limit the stimulation frequency of a single target location to 0.5 Hz, where possible. For higher stimulation frequencies, the decaying response amplitude has to be taken into account.

Effective beam diameter

The effective size of the laser beam, i.e., the area in which high levels of glutamate are released by a single shot, is an important measure for multi-site, dynamic photo stimulation. Together with the maximum stimulation frequency for a single spot, it gives an estimate of the overall maximum stimulation frequency that can be applied to a given area of slice tissue. In our setup, the laser beam was focused to a spot diameter of ~50 μm in the plane of the recording chamber bottom. The physiologically effective beam diameter, however, might be substantially larger because of light scattering in the tissue and diffusion of uncaged neurotransmitter. We tested the physiologically effective beam size with single light pulses applied at different distances from the soma of intracellularly recorded pyramidal layer V neurons. Scans with a step size of 100 μm along lines perpendicular to the apical dendrite of each pyramidal cell revealed for all calibrated cells ($n = 3$) an effective beam diameter of <200 μm for spike generation and of ~400–500 μm for the generation of EPSP-like depolarizations at moderate laser intensities. A typical example for a layer V pyramidal cell is shown in Fig. 4. The observed subthreshold responses clearly depended on the morphological characteristics of the studied neurons: the long, apical dendrite of the pyramidal cells lead to a strongly nonisotropic profile. The physiologically effective beam size is determined by the effective overlap of the light spot and the branching area of the dendrite. While morphology was clearly reflected in the subthreshold responses, spiking was almost exclusively provoked by means of direct somatic stimulation, except for strong stimulation of the dendritic tuft in layer I. Two important parameters can be extracted from these calibration measurements: first, the effective beam size for subthreshold responses gives an estimate of the area around the intracellularly recorded neuron that should be spared from illumination to avoid direct dendritic stimulation of the cell in which the activity-dependent phenomena were to be studied. Second, the effective beam size for suprathreshold stimulation, i.e., for spike generation in cells presynaptic to the intracellularly recorded cell, determines the spatial resolution for the generation of functional maps. From these maps, the sites for dynamic stimulation of presynaptic neurons were ultimately chosen.

Increasing the laser power increased the radius around the soma within which photo stimulation became suprathreshold with respect to action potential generation (cf. curves for 15 and 25 mW, Fig. 4). Laser power, thus provides an important parameter for controlling the effective beam diameter or, in

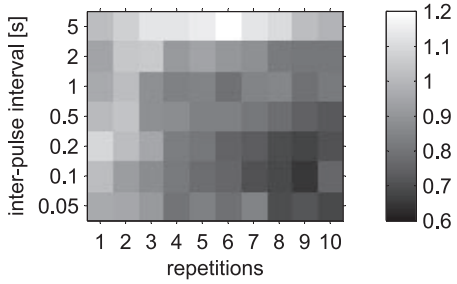

FIG. 3. Decay of extracellular population responses during repeated stimulation of the same target position. An extracellular recording electrode was inserted into tissue in layer III or V, and regular trains of 10 laser pulses were applied to tissue located at the tip of that electrode. Population responses were quantified as response amplitude (see Fig. 2) while varying the interpulse interval (IPI) from train to train. Results from different neurons ($n = 5$) were normalized to the mean of the 1st responses of applied trains (scalebar: response amplitude in relative units).

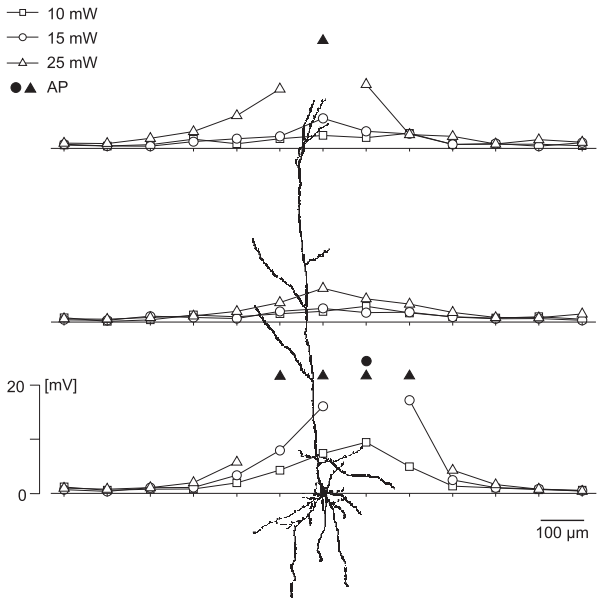

FIG. 4. Physiologically effective beam size at a target location that is directly stimulated by laser uncaging. Single light pulses were applied to the locations specified by the axis tics. Amplitudes of subthreshold postsynaptic potentials are shown as open symbols; closed symbols correspond to locations where a single shot elicited an action potential (PD = 24 ms). While the subthreshold response profiles for different laser intensities showed a similar shape, the thresholding mechanism of action potential generation has a strong effect on effective width for suprathreshold responses (filled symbols). Laser power is thus an important parameter to control the number of presynaptic neurons activated by a single laser pulse.

other words, the number of presynaptic neurons activated by a single light pulse. In the experimental system described here, laser power was limited to a maximum of 40 mW, requiring pulse durations of ≥4 ms for spike generation in presynaptic cells. We did not use higher laser power to avoid photo damage of the tissue: while extensive stimulation of the same target location (several hundred shots of a few milliseconds duration) with high laser power lead to signs of photo damage, namely diffraction index changes reminiscent of spreading depression, these effects were not observed when laser power was <40 mW (data not shown).

Functional mapping of presynaptic sites

To find neurons with functional connections to the target cell (here, layer V pyramidal cells in the somatosensory cortex), we acquired a functional map for the intracellularly recorded cell by scanning the tissue with single light pulses. Target locations were placed on the nodes of a grid with typically 100-μm internode distance, covering 1 mm of neocortical tissue to the left and to the right of the intracellularly recorded cell. This scanning procedure yielded a response map with mixed responses from synaptic and direct stimulations. The response to each shot was quantified in terms of amplitude of the postsynaptic current, its rise time, and its latency with respect to stimulation onset. Input through functional projections could be distinguished from direct dendritic stimulation based on these characteristics of the postsynaptic currents (see also Shepherd et al. 2003). Only those stimulus locations that clearly produced purely synaptic currents without any contribution from direct stimulation of the postsynaptic cell were used for further stimulations. Plotting intracellularly measured PSC amplitudes at the corresponding presynaptic stimulation location yielded a functional connectivity map of the target cell (Fig. 5*A, left*). As a control, functional mapping was repeated at the end of the experiment in the presence of TTX (4 μM). The residual responses were considered to result from direct dendritic stimulations of the postsynaptic cell (Fig. 5*A, right*). In the connectivity map in the *left panel*, the target locations corresponding to direct stimulations were left blank. The TTX control confirmed that the criteria used for selection of purely synaptic input were appropriate (cf. Fig. 5, *A* and *B*).

Reliability and temporal precision of postsynaptic responses

Our method was designed to generate controlled synaptic input into the postsynaptic cell, and thereby to provide us with the means to study issues of signal integration under defined activity conditions. It was, thus important *1*) to reliably induce an action potential in the presynaptic cell and *2*) to measure the temporal precision and amplitude variability of the respective postsynaptic events. To quantify the variability of stimulated synaptic transmission, we chose presynaptic sites whose stimulation produced clear synaptic responses in the target cell (no components from direct dendritic stimulation) and repeated the stimulation several times. From the input map shown in Fig. 5*A* we chose seven presynaptic stimulation sites of which six entered our statistics. The responses to repeated stimulation at four different sites are shown in Fig. 5*B*. At these sites, all 11 repetitions were successful. The rightmost response clearly indicates multiple presynaptic spikes, or a presynaptic burst of action potentials, as are likely to occur for higher stimulation energies (see Fig. 2). Such multiple-event responses were excluded from our statistical analysis. The reliability, i.e., the percentage of successful stimulations of presynaptic neurons, increased as a function of the trial-averaged EPSC amplitude to 100% for EPSCs larger than 20 pA (Fig. 5*C*, *left*). Relative trial-to-trial variability, as measured by the CV of the PSC amplitude, was smallest for the largest PSCs, where the SD made up for only a small fraction of the mean amplitude (Fig. 5*C, middle*).

The temporal precision of PSC arrival was quantified by the SD of the latency measured from stimulus onset (i.e., shutter opening) to PSC onset. It ranged from shorter than a millisecond for short latencies to <3 ms for the longest ones (Fig. 5*C, right*). This is comparable with the high temporal precision obtained for AP generation by somatic injection of noise currents (Mainen and Sejnowski 1995). In all cell pairs, latencies were in the range between 7 and 17 ms. Analysis of the spike timings of extracellularly measured population responses, as recorded for the characterization of the presynaptic responses (Fig. 2), revealed that latencies between stimulus onset and PSC were mostly caused by delays in spike initiation (data not shown).

Reliability of information transfer between pyramidal cells of the neocortex

The transfer of information in neuronal networks heavily depends on the precision and reliability with which signals are transferred from one cell to the next and on the details of signal integration within a single cell. In this chain of events, synaptic transmission, postsynaptic dendritic integration, and spike gen-

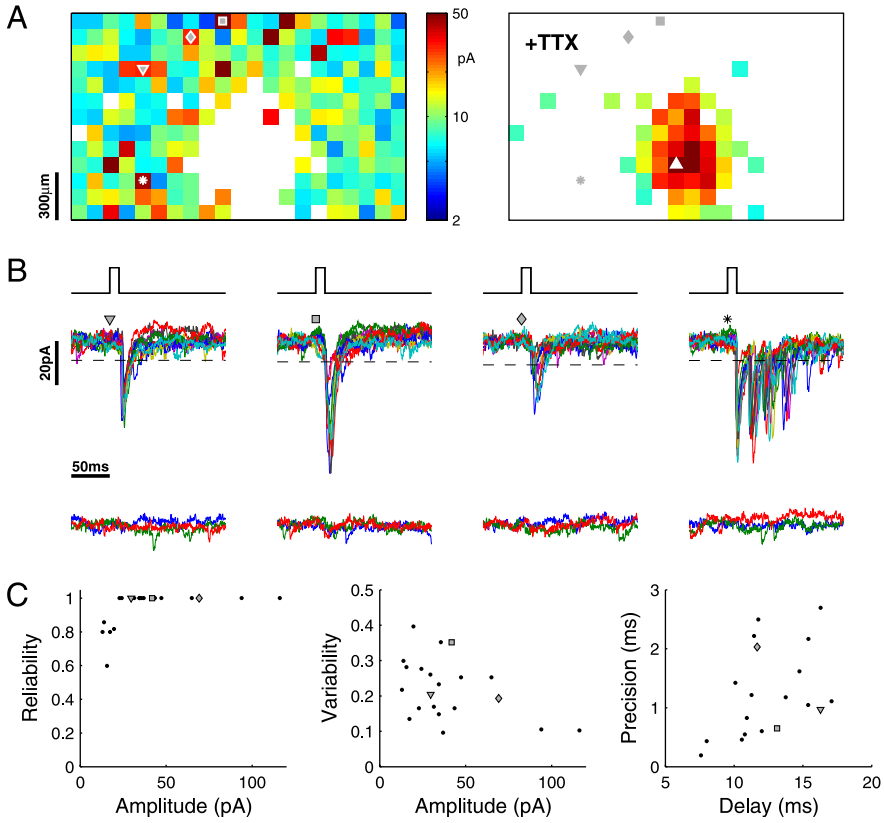

FIG. 5. Postsynaptic currents after single-shot stimulation of presynaptic target sites. *A*: functional input map for the intracellularly recorded cell (upright white triangle) was acquired by probing the surrounding slice tissue with single shots of 12 ms and 35 mW laser power. Amplitudes of postsynaptic responses are displayed at the respective presynaptic stimulation site. *Right*: residual responses exceeding a certain threshold after incubation with TTX (20 min with 4 μM). Because these responses cannot represent activation of functional projections, they are considered reactions to direct stimulation of the recorded cell. *Left*: corresponding positions are left blank, leaving a map of the presynaptic sites available for purely synaptic stimulation of the intracellularly recorded cell. Samples of postsynaptic responses are shown in *B*, where traces correspond to stimulation at target positions indicated by the corresponding symbols in the functional map. To test reliability, reproducibility, and precision of postsynaptic responses, presynaptic stimulation was repeated 11 times (IPI $>$ 2 min). *Bottom traces* in *B* show absence of postsynaptic responses to stimulation of the same targets after TTX incubation. *C*: summary of data from 4 similar experiments, at a total of 21 sites in 4 neurons (number of repetitions per target location between 7 and 11). Reliability measures relative number of successful stimulations, leading to a detectable postsynaptic current (PSC). Variability is measured by the CV of peak amplitude of PSCs across trials. We obtained values in the range of 10–40%. Temporal precision of PSC onset times was better than 3 ms of trial-to-trial SD.

eration in the postsynaptic cell are, in general, considered the most influential processes. Each of these steps alone has been studied in detail in cultured cells, in the slice preparation, and in vivo. With the new method of dynamic photo stimulation we can now, for the first time, generate sufficiently intense synaptic input into a pyramidal neuron in an acute slice to study the reliability of all these steps simultaneously at the single cell level. To show this, we show samples of postsynaptic voltage responses to repeated stimulation of a cortical layer V pyramidal cell with the same spatio-temporal input pattern. We first selected as many presynaptic stimulation locations as possible (in this experiment, $n = 34$) that produced clear EPSC-shaped responses in the postsynaptic cell based on its functional connectivity map (Fig. 5). A random sequence of 400 successive stimulations of the selected 34 positions was generated and saved for multiple replay (frozen noise). The interval statistics of the train was in accordance with a dead-time Poisson process. The mean frequency was 40 stimulations per second, implying a mean interstimulus interval of 25 ms. We imposed a minimum interval (dead-time) of 10 ms between successive stimulations, fully covering the pulse duration of 5 ms. Figure 6*A* shows the postsynaptic membrane potential fluctuations resulting from such a stimulus train. Immediately after stimulus onset ($t = 0$), the membrane potential exhibited fast fluctuations because of the synaptic input, which ceased after the stimulation sequence was stopped and the membrane potential returned to its resting value. Stimulation with the same sequence after incubation with TTX (4 μM) elicited little residual activity (Fig. 6*A*, gray curve), showing that the evoked responses were not strictly synaptic but contained some contributions from direct dendritic simulation of the target cell. The fast components of the membrane potential deflections, however, proved to be of synaptic origin.

We replayed the same stimulation pattern two more times and observed that the entire membrane potential time-course in the postsynaptic neuron was reproduced with surprisingly high accuracy, as is shown in the overlay of all three consecutive voltage traces in Fig. 6*B*. From each single trial, we had subtracted the corresponding mean resting potential as measured during 1 s before stimulation onset, as well as the residual signal obtained under TTX block. To quantify the reproducibility of subthreshold membrane potential fluctuations in different repetitions we measured the cross-correlation among any pair of voltage traces after cutting out the spikes (see METHODS). The average cross-correlation (CC) as a function of relative time lag is depicted in Fig. 6*C* (black curve), with a maximum correlation coefficient of CC = 0.87 at lag zero. The shape of the CC function resembled very well that of the average autocorrelation function (gray curve). The width of the central peak mainly reflects the membrane time constant of the neuron. The relative timing of the postsynaptic spike responses across trials also exhibited a precision in the millisecond range (mean SD = 1.3 ms, $n = 3$, see METHODS), comparable with the precision measured in somatic noise current injection experiments.

DISCUSSION

We have presented a new method to induce tightly controlled, vivid synaptic activity into single cells within an acute brain slice using the dynamic, photolytic release of the excitatory transmitter glutamate. To achieve this, we extended

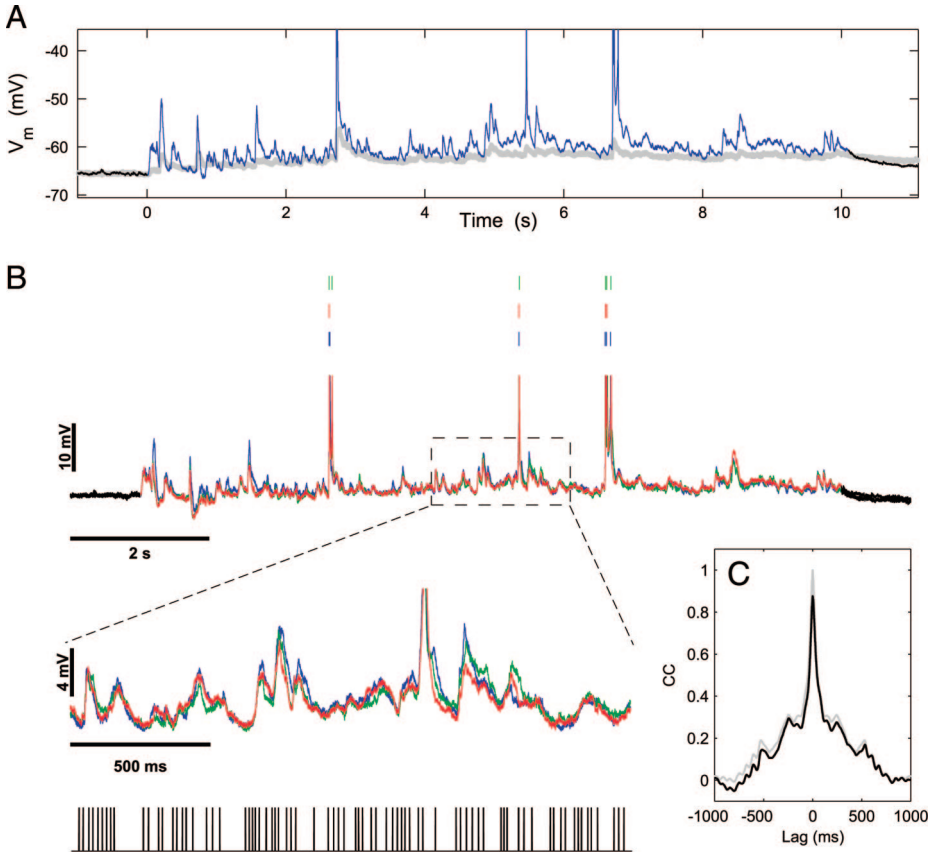

FIG. 6. Vivid postsynaptic activity generated with dynamic photo stimulation in an acute brain slice. Thirty-four target sites, at which stimulation produced postsynaptic responses that were considered purely synaptic, were chosen from a functional input map. These sites were stimulated in random order and with irregular temporal sequence at an average frequency of 40 Hz. *A*: resulting fluctuations of postsynaptic membrane potential (blue trace) and after incubation with TTX (4 μM, gray trace) in response to exactly the same stimulation sequences. Residual activity under TTX shows that stimulation also included some direct illumination of the dendrite of the intracellularly recorded cell. *B*: to test reliability of signal transfer between neurons, the same stimulation sequence was applied 3 times (>2 min between trials). From each trace, residual activity under TTX and mean membrane potential during a baseline period were subtracted. Overlay of resulting traces showed remarkably little variation between trials, which also applied to timing of action potentials (colored tic marks). *Bottom trace* shows a zoom-in of the box in the *top trace*. Black tics are times of shutter opening. Reproducibility of membrane potential fluctuations is quantified in *C* by averaged cross-correlation function for all pairs of trials (black curve; action potentials removed before analysis). Gray curve shows averaged auto-correlation function for all 3 trials.

and improved the method of neurotransmitter uncaging by developing a setup allowing fast and precise positioning of a focused laser beam to any target within a conventional in vitro recording chamber. Because of the wide spatial stimulation range, we could avoid direct stimulation of the postsynaptic cell and, instead, generate synaptic activity through the activation of distant, presynaptic target cells. This way, we circumvent problems of out of focus neurotransmitter release and, in addition, avoid unwanted, extrasynaptic receptor activation in the intracellularly recorded, postsynaptic cell. Our system allows to generate well-defined spatio-temporal patterns of synaptic activity by employing a variety of axonal projections that all terminate on the postsynaptic cell.

Advantages compared with existing setup designs for dynamic photo stimulation

The design of a setup for dynamic photo stimulation very much depends on whether postsynaptic sites should be stimulated directly by neurotransmitter uncaging or by activation of functional projections from other neurons. Direct dendritic stimulation requires a strongly focused beam (ideally suitable for the stimulation of single postsynaptic sites, or synapses) and a high spatial resolution of beam positioning. Both can, in principle, be achieved by projecting the light through the lens of a microscope. However, to obtain the possibility of dynamic stimulation, it has to be combined with a system for rapid target positioning. Such a system has been described (Bullen and Saggau, 1999), but this objective-based approach imposes severe limitations. The stimulation area is confined to the field of view of the objective (usually $<200 \times 200$ μm) and substantial power loss in the optical pathway (usually in the range of >90%) has to be accepted, raising the need for comparatively strong and thus expensive laser light sources. Recently, an objective-based laser stimulation setup with low magnification for functional mapping studies was described (Shepherd et al. 2003), which should, in principle, be suitable for dynamic photo stimulation through functional projections. Surprisingly, the authors showed a comparatively poor reproducibility of postsynaptic currents during repetitive stimulation. In contrast to our experiments, a pulsed laser and a different caging group for the caged glutamate was used in this study. In how far these differences or other details, like the comparatively short pulse duration (1 ms) or the lower age of animals impaired the reproducibility, remains unclear. In any case, even with a low-power objective, the spatial projection range of the laser beam is limited to $\sim 800 \times 800$ μm, a strong laser source has to be used, and the beam has to pass a layer of buffer before it reaches the tissue and can thus release substantial amounts of transmitter in the superfusate. Another disadvantage of introducing the laser light from above is that every recording electrode introduced into the slice shades the tissue underneath from irradiation, effectively reducing the area available for photo stimulation in an uncontrolled manner. While such shading may be acceptable for connectivity studies with only one intracellular electrode, it turns into a problem when two or more electrodes are used, as in the case of multiple-site recordings, paired recordings, or parallel intra- and extracellular recordings. The special design of the experimental setup presented in this study avoids these problems by introducing the laser light from below, through the bottom of the recording chamber, while

conserving the advantageous aspects of a mirror-based laser deflection device (high precision and speed).

Control parameters for dynamic photo stimulation

The results of our calibration measurements show the capabilities of dynamic photo stimulation for the generation of trains of both well-separated and overlapping PSCs. They especially show that it is possible to generate PSCs with a reliability close to 100%, with a precision in the range from submillisecond up to <3 ms, and with a very good amplitude variability. This variability most likely reflects, apart from measurement noise and channel noise, to the greater part the variability intrinsic to synaptic transmission, i.e., the variable number of released vesicles per synaptic transmission event. As the evaluation of the single-shot responses show, the use of a continuous laser source with a variable shutter, as opposed to a flash-lamp, provides the means to shape the presynaptic response in terms of onset latency and temporal structure of the presynaptic spiking. In principle, pulse duration could be adjusted individually for each presynaptic target location, if, for example, multiple PSCs (as shown in Fig. 5*B, right trace*) were to be avoided or PSCs with certain latencies were to be generated. In addition, our calibration measurements show that comparatively high laser power is needed to evoke presynaptic spikes if pulse duration is short. A possible explanation for this is the comparatively long rise time of currents generated by direct, somatic photo stimulation (~10 ms; data not shown). This rise time presumably depends on a number of parameters, such as removal rate of free glutamate in the tissue, receptor subtype distribution and density, and the stability of the caging group used. The advantages of a continuous laser source for the adjustment of strength and temporal structure of the presynaptic activity justify the comparatively high costs compared with a UV flash-lamp.

Generation of vivid postsynaptic activity

The generation of vivid synaptic activity in an intracellularly recorded cell can be considered the most challenging application of our new stimulation technique, because it critically depends on a number of factors. First of all, it requires a rich connectivity preserved within the acute brain slice preparation. Recent work with highly focused photolysis of caged compounds has revealed a wealth of short- and long-range functional synaptic connections within acute neocortical slices (for review, see Callaway and Yuste 2002). Such measurements deliver direct quantifications of the density and preferred direction of intracortical projections for defined brain areas. An easier estimate for the suitability of slice tissue for dynamic photo stimulation could be its responsiveness to electrically evoked polysynaptic ensemble activity: While in coronal sections of auditory and somato-sensory cortices, electrical stimulation can evoke transient ensemble activity, the protocol fails in other brain areas (Wu et al. 2001), suggesting a lower number of functional axonal projections. Connectivity might also be influenced by the choice of the cutting angle during the slicing procedure, leaving different fractions of intracortical projections intact (Hishida et al. 2003; Malach et al. 1997).

For successful exploitation of functional projections in our setup for the generation of vivid postsynaptic activity, these projections have to extend over a minimal distance, which is mainly determined by the physiologically effective beam diameter, i.e., the zone around the postsynaptic cell where illumination leads to direct stimulation of its dendrites. Even though in vivo studies showed that excitatory, monosynaptic connections could be found between cells with a mutual distance of 3 mm or more (Matsumura et al. 1996), the projections of inhibitory neurons are usually more locally confined (Budd and Kisvarday 2001; Kisvarday et al. 2002). The latter is a likely explanation for the fact that purely postsynaptic inhibitory currents were only rarely observed in our experiments. For studies that require inhibitory inputs or a higher number of discrete presynaptic excitatory sites, a reduction of the effective beam size with respect to spike generation could be achieved by a stronger focusing of the laser beam. In how far this will be sufficient to achieve input rates that come close to those in the in vivo situation remains to be evaluated. In any case, the maximum input rate is technically limited to ~300 Hz by the speed of the mirrors, assuming a pulse length of 1 ms. The average number of synapses is estimated to range from 5.000 to 13.000 per cell (for layers 2/3 and layer 5 neocortical pyramidal cells, respectively; Binzegger et al. 2004), whereas the average spike rate in vivo is usually assumed to be between 5 and 10 Hz. This would yield an average input rate in the range of 25–130 kHz, which is way beyond the capabilities of our setup. However, these estimates are very coarse and do not necessarily reflect the real situation in vivo: it is unclear, how many of the morphologically identified synapses are active, and recent reports on in vivo patch-clamp recordings suggest that some neurons may, in fact, have a very low spontaneous firing rate (<0.1 Hz; Brecht and Sakmann 2002).

An important finding from the calibration measurements is that the use of our setup for high-frequency stimulation is slightly complicated by the decaying responses to repeated stimulation of the same spot for IPIs between 2 s and 500 ms, as shown in Fig. 3. The reason for this behavior is most likely a combination of different mechanisms, such as free glutamate accumulation, re-uptake and diffusion, receptor desensitization, and driving force changes within the target cell. Therefore to predict the response to a train of pulses with short IPIs, the history of shots to each single target position has to be taken into account according to the calibration measurements (Fig. 3). For the question of reliability of signal transfer, however, predictability of the response from the single-shot responses plays only a minor role: as is shown in Fig. 6, these effects do not influence the reproducibility between repetitions of an identical stimulation sequence.

Fields of application

The method of dynamic photo stimulation through functional projections in acute brain slices presented in this paper is of particular interest for the study of postsynaptic mechanisms that critically depend on the details of the temporal activation pattern of synaptic input. One particular issue that has been raised in this context concerns the reliability and precision with which a neuron can respond to dynamic input patterns (Mainen and Sejnowski 1995; Nowak et al. 1997). Here, we presented a way of how this question could be approached experimentally in vitro. Our results show that the same stimulus train of

presynaptic neurons not only elicited spike responses in the postsynaptic cell with a high temporal precision, but also evoked subthreshold membrane potential deflections with a high reproducibility. This suggests that synaptic transmission, single cell processing of inputs and subsequent generation of action potentials are all highly reliable processes. Our preliminary data are in line with results from in vivo studies in sensory systems, which provide accumulating evidence that spike train responses are repeated with millisecond precision in response to the repeated presentation of adequate dynamic stimuli (Aertsen et al. 1979; Elhilali et al. 2004; Jones et al. 2004; Theunissen et al. 2000).

Reliability of the spike generator would be a central prerequisite for the viability of temporal coding in the neocortex. Another necessary requirement at the single-cell level would be a mechanism for efficient transformation of correlated input from ensembles of presynaptic neurons into precisely timed spike output (Abeles et al. 1993; for review, see Salinas and Sejnowski 2001). Based on theoretical work, it was postulated that such near-coincident inputs have to arrive at the postsynaptic cell with a temporal spread that is clearly below the leak time constant of the membrane (Diesmann et al. 1999; Kuhn et al. 2003; Salinas and Sejnowski 2000). The efficacy of such correlated inputs has also been studied in experimental work in vitro using current injection. The results suggested that pulse packets comprising 5–50 correlated inputs could be very effective in driving a neuron to firing threshold (Nawrot et al. 2003; Reyes 2003). With our setup, we are capable of producing synaptic events with a controlled degree of coherence: in any set of presynaptic target locations that produce postsynaptic PSCs, different delays of PSC onset relative to stimulation onset will allow us to construct a compound PSC with well-defined temporal relations. Because our method employs functional, spatially distributed synapses, experiments can be performed in a much more realistic setting than those using somatic current injection, where dendritic morphology, spatial distribution of synapses, and dendritic integration are neglected.

Considering dendritic morphology suggests another interesting set of questions where experimental approaches with dynamic photo stimulation have the potential to provide a more realistic picture than somatic or dendritic current injections: how exactly do dendritic morphology and active dendritic conductances influence the integration properties of neocortical pyramidal cells? The importance of active dendrites for signal integration has increasingly been acknowledged in recent years (Häusser et al. 2000; Magee and Cook 2000; for review, see Williams and Stuart 2003), but up to now, the type of synaptic activity leading to the activation of the respective conductances in vivo could only be approximated in vitro by injections of currents or conductances at somatic or dendritic locations using just a few electrodes. Dynamic photo stimulation, in contrast, provides the first experimental paradigm that allows the controlled activation of a large number of real synapses on a single postsynaptic cell in vitro. To reveal the location of the active synapses, calcium imaging, or multiple-site electrode recordings from the postsynaptic cell can be combined with dynamic photo stimulation (Schiller et al. 2000).

As a last example for the potential use of dynamic photo stimulation, we would like to point to questions related to synaptic plasticity. Besides the fact that a high number of different synapses on the same postsynaptic cell could be probed simultaneously for plasticity phenomena, dynamic photo stimulation opens new experimental access to questions that could, so far, only be addressed in modeling studies. One example is "synaptic scaling," a mechanism that was proposed to regulate the overall sum of synaptic weights within a given cell. Such a mechanism could be necessary to prevent an overexcitation of a postsynaptic cell that was subjected to intense synaptic potentiation of many synapses (Abbott and Nelson 2000). This and related processes cannot be studied experimentally with conventional in vivo or in vitro models, because it would require the controlled induction of synaptic potentiation in many synapses of the same cell. With dynamic photo stimulation, it is particularly easy to pair synaptic activity with action potentials elicited by somatic current injection to induce spike-timing dependent plasticity and even tetanic stimulation of presynaptic neurons could be realized with accordingly adjusted stimulation parameters.

Taken together, dynamic photo stimulation provides us with a powerful new tool to experimentally study the dynamic interplay between the integrative properties of single neurons and the extent and spatio-temporal structure of its synaptic inputs. It will allow us to obtain a more realistic picture of the mechanisms involved in information processing in single cells at multiple levels, from the synapse up to general questions regarding the effect of the space-time-structure of inputs on signal integration.

ACKNOWLEDGMENTS

We thank the team of our mechanical and electrical workshop, in particular D. Schächtele and J. Schmidt, for great competence in finding technical solutions during the development of the setup. Furthermore, we thank H. Gavrilova for excellent neuron reconstructions, as well as H. Keiser (Laser-Scanning-Keiser, Stallikon, Switzerland) for advice and support and B. Kampa for contributions during the initial phase of the project.

GRANTS

This work was supported by the German Research Council (Deutsche Forschungsgemeinschaft-Sonderforschungsbereich 505).

REFERENCES

Abbott LF and Nelson SB. Synaptic plasticity: taming the beast. *Nat Neurosci* 3: 1178–1183, 2000.

Abeles M, Bergman H, Margalit E, and Vaadia E. Spatiotemporal firing patterns in the frontal cortex of behaving monkeys. *J Neurophysiol* 70: 1629–1638, 1993.

Aertsen AM, Smolders JW, and Johannesma PI. Neural representation of the acoustic biotope: on the existence of stimulus-event relations for sensory neurons. *Biol Cybern* 32: 175–185, 1979.

Azouz R and Gray CM. Cellular mechanisms contributing to response variability of cortical neurons in vivo. *J Neurosci* 19: 2209–2223, 1999.

Azouz R and Gray CM. Dynamic spike threshold reveals a mechanism for synaptic coincidence detection in cortical neurons in vivo. *Proc Natl Acad Sci USA* 97: 8110–8115, 2000.

Bernander O, Douglas RJ, Martin KA, and Koch C. Synaptic background activity influences spatiotemporal integration in single pyramidal cells. *Proc Natl Acad Sci USA* 88: 11569–11573, 1991.

Binzegger T, Douglas RJ, and Martin KA. A quantitative map of the circuit of cat primary visual cortex. *J Neurosci* 24: 8441–8453, 2004.

Bischofberger J, Geiger JR, and Jonas P. Timing and efficacy of Ca^{2+} channel activation in hippocampal mossy fiber boutons. *J Neurosci* 22: 10593–10602, 2002.

Brecht M and Sakmann B. Dynamic representation of whisker deflection by synaptic potentials in spiny stellate and pyramidal cells in the barrels and septa of layer 4 rat somatosensory cortex. *J Physiol* 543: 49–70, 2002.

Budd JM and Kisvarday ZF. Local lateral connectivity of inhibitory clutch cells in layer 4 of cat visual cortex (area 17). *Exp Brain Res* 140: 245–250, 2001.

Bullen A and Saggau P. High-speed, random-access fluorescence microscopy. II. Fast quantitative measurements with voltage-sensitive dyes. *Biophys J* 76: 2272–2287, 1999.

Callaway EM and Katz LC. Photostimulation using caged glutamate reveals functional circuitry in living brain slices. *Proc Natl Acad Sci USA* 90: 7661–7665, 1993.

Callaway EM and Yuste R. Stimulating neurons with light. *Curr Opin Neurobiol* 12: 587–592, 2002.

Dalva MB and Katz LC. Rearrangements of synaptic connections in visual cortex revealed by laser photostimulation. *Science* 265: 255–258, 1994.

Dantzker JL and Callaway EM. Laminar sources of synaptic input to cortical inhibitory interneurons and pyramidal neurons. *Nat Neurosci* 3: 701–707, 2000.

Destexhe A and Pare D. Impact of network activity on the integrative properties of neocortical pyramidal neurons in vivo. *J Neurophysiol* 81: 1531–1547, 1999.

Destexhe A, Rudolph M, and Pare D. The high-conductance state of neocortical neurons in vivo. *Nat Rev Neurosci* 4: 739–751, 2003.

Diesmann M, Gewaltig MO, and Aertsen A. Stable propagation of synchronous spiking in cortical neural networks. *Nature* 402: 529–533, 1999.

Dodt H, Eder M, Frick A, and Zieglgänsberger W. Precisely localized LTD in the neocortex revealed by infrared-guided laser stimulation. *Science* 286: 110–113, 1999.

Dodt HU, Schierloh A, Eder M, and Zieglgänsberger W. Circuitry of rat barrel cortex investigated by infrared-guided laser stimulation. *Neuroreport* 14: 623–627, 2003.

Dodt HU and Zieglgänsberger W. Visualizing unstained neurons in living brain slices by infrared DIC-videomicroscopy. *Brain Res* 537: 333–336, 1990.

Durstewitz D, Seamans JK, and Sejnowski TJ. Neurocomputational models of working memory. *Nat Neurosci* 3: 1184–1191, 2000.

Elhilali M, Fritz JB, Klein DJ, Simon JZ, and Shamma SA. Dynamics of precise spike timing in primary auditory cortex. *J Neurosci* 24: 1159–1172, 2004.

Godwin DW, Che D, O'Malley DM, and Zhou Q. Photostimulation with caged neurotransmitters using fiber optic lightguides. *J Neurosci Methods* 73: 91–106, 1997.

Hardingham GE, Fukunaga Y, and Bading H. Extrasynaptic NMDARs oppose synaptic NMDARs by triggering CREB shut-off and cell death pathways. *Nat Neurosci* 5: 405–414, 2002.

Häusser M, Spruston N, and Stuart GJ. Diversity and dynamics of dendritic signaling. *Science* 290: 739–744, 2000.

Hishida R, Hoshino K, Kudoh M, Norita M, and Shibuki K. Anisotropic functional connections between the auditory cortex and area 18a in rat cerebral slices. *Neurosci Res* 46: 171–182, 2003.

Ho N and Destexhe A. Synaptic background activity enhances the responsiveness of neocortical pyramidal neurons. *J Neurophysiol* 84: 1488–1496, 2000.

Horikawa K and Armstrong WE. A versatile means of intracellular labeling: injection of biocytin and its detection with avidin conjugates. *J Neurosci Methods* 25: 1–11, 1988.

Jagadeesh B, Wheat HS, and Ferster D. Linearity of summation of synaptic potentials underlying direction selectivity in simple cells of the cat visual cortex. *Science* 262: 1901–1904, 1993.

Jones LM, Lee S, Trageser JC, Simons DJ, and Keller A. Precise temporal responses in whisker trigeminal neurons. *J Neurophysiol* 92: 665–668, 2004.

Kamondi A, Acsady L, and Buzsaki G. Dendritic spikes are enhanced by cooperative network activity in the intact hippocampus. *J Neurosci* 18: 3919–3928, 1998.

Kandler K, Katz LC, and Kauer JA. Focal photolysis of caged glutamate produces long-term depression of hippocampal glutamate receptors. *Nat Neurosci* 1: 119–123, 1998.

Katz LC and Dalva MB. Scanning laser photostimulation: a new approach for analyzing brain circuits. *J Neurosci Methods* 54: 205–218, 1994.

Kisvarday ZF, Ferecsko AS, Kovacs K, Buzas P, Budd JM, and Eysel UT. One axon - multiple functions: specificity of lateral inhibitory connections by large basket cells. *J Neurocytol* 31: 255–264, 2002.

Kötter R, Staiger JF, Zilles K, and Luhmann HJ. Analysing functional connectivity in brain slices by a combination of infrared video microscopy, flash photolysis of caged compounds and scanning methods. *Neuroscience* 86: 265–277, 1998.

Kuhn A, Aertsen A, and Rotter S. Higher-order statistics of input ensembles and the response of simple model neurons. *Neural Comput* 15: 67–101, 2003.

Kuhn A, Aertsen A, and Rotter S. Neuronal integration of synaptic input in the fluctuation-driven regime. *J Neurosci* 24: 2345–2356, 2004.

Larkum ME and Zhu JJ. Signaling of layer 1 and whisker-evoked Ca^{2+} and Na^{+} action potentials in distal and terminal dendrites of rat neocortical pyramidal neurons in vitro and in vivo. *J Neurosci* 22: 6991–7005, 2002.

Larkum ME, Zhu JJ, and Sakmann B. Dendritic mechanisms underlying the coupling of the dendritic with the axonal action potential initiation zone of adult rat layer 5 pyramidal neurons. *J Physiol* 533: 447–466, 2001.

Leger JF, Stern EA, Aertsen A, and Heck D. Synaptic integration in rat frontal cortex shaped by network activity. *J Neurophysiol* 93: 281–293, 2005.

Magee JC and Cook EP. Somatic EPSP amplitude is independent of synapse location in hippocampal pyramidal neurons. *Nat Neurosci* 3: 895–903, 2000.

Mainen ZF and Sejnowski TJ. Reliability of spike timing in neocortical neurons. *Science* 268: 1503–1506, 1995.

Malach R, Schirman TD, Harel M, Tootell RB, and Malonek D. Organization of intrinsic connections in owl monkey area MT. *Cereb Cortex* 7: 386–393, 1997.

Margulis M and Tang CM. Temporal integration can readily switch between sublinear and supralinear summation. *J Neurophysiol* 79: 2809–2813, 1998.

Markram H, Wang Y, and Tsodyks M. Differential signaling via the same axon of neocortical pyramidal neurons. *Proc Natl Acad Sci USA* 95: 5323–5328, 1998.

Matsumura M, Chen D, Sawaguchi T, Kubota K, and Fetz EE. Synaptic interactions between primate precentral cortex neurons revealed by spike-triggered averaging of intracellular membrane potentials in vivo. *J Neurosci* 16: 7757–7767, 1996.

Nawrot MP, Pistohl T, Schrader S, Hehl U, Rodriguez V, and Aertsen A. Embedding living neurons into simulated neural networks. *Proc EMBS Neural Engin* 229–232, 2003.

Nowak LG, Sanchez-Vives MV, and McCormick DA. Influence of low and high frequency inputs on spike timing in visual cortical neurons. *Cereb Cortex* 7: 487–501, 1997.

Oviedo H and Reyes AD. Boosting of neuronal firing evoked with asynchronous and synchronous inputs to the dendrite. *Nat Neurosci* 5: 261–266, 2002.

Pare D, Shink E, Gaudreau H, Destexhe A, and Lang EJ. Impact of spontaneous synaptic activity on the resting properties of cat neocortical pyramidal neurons in vivo. *J Neurophysiol* 79: 1450–1460, 1998.

Pettit DL, Wang SS, Gee KR, and Augustine GJ. Chemical two-photon uncaging: a novel approach to mapping glutamate receptors. *Neuron* 19: 465–471, 1997.

Reyes AD. Synchrony-dependent propagation of firing rate in iteratively constructed networks in vitro. *Nat Neurosci* 6: 593–599, 2003.

Salinas E and Sejnowski TJ. Impact of correlated synaptic input on output firing rate and variability in simple neuronal models. *J Neurosci* 20: 6193–6209, 2000.

Salinas E and Sejnowski TJ. Correlated neuronal activity and the flow of neural information. *Nat Rev Neurosci* 2: 539–550, 2001.

Schiller J, Major G, Koester HJ, and Schiller Y. NMDA spikes in basal dendrites of cortical pyramidal neurons. *Nature* 404: 285–289, 2000.

Shepherd GM, Pologruto TA, and Svoboda K. Circuit analysis of experience-dependent plasticity in the developing rat barrel cortex. *Neuron* 38: 277–289, 2003.

Stern EA, Maravall M, and Svoboda K. Rapid development and plasticity of layer 2/3 maps in rat barrel cortex in vivo. *Neuron* 31: 305–315, 2001.

Tamas G, Szabadics J, and Somogyi P. Cell type- and subcellular position-dependent summation of unitary postsynaptic potentials in neocortical neurons. *J Neurosci* 22: 740–747, 2002.

Theunissen FE, Sen K, and Doupe AJ. Spectral-temporal receptive fields of nonlinear auditory neurons obtained using natural sounds. *J Neurosci* 20: 2315–2331, 2000.

Wang SS and Augustine GJ. Confocal imaging and local photolysis of caged compounds: dual probes of synaptic function. *Neuron* 15: 755–760, 1995.

Williams SR and Stuart GJ. Dependence of EPSP efficacy on synapse location in neocortical pyramidal neurons. *Science* 295: 1907–1910, 2002.

Williams SR and Stuart GJ. Role of dendritic synapse location in the control of action potential output. *Trends Neurosci* 26: 147–154, 2003.

Wu JY, Guan L, Bai L, and Yang Q. Spatiotemporal properties of an evoked population activity in rat sensory cortical slices. *J Neurophysiol* 86: 2461–2474, 2001.

Zhu JJ and Connors BW. Intrinsic firing patterns and whisker-evoked synaptic responses of neurons in the rat barrel cortex. *J Neurophysiol* 81: 1171–1183, 1999.